ISSN 1063-7834, Physics of the Solid State, 2010, Vol. 52, No. 8, pp. 1680–1687. © Pleiades Publishing, Ltd., 2010.
Original Russian Text © M.M. Otrokov, S.A. Ostanin, A. Ernst, V.M. Kuznetsov, E.V. Chulkov, 2010, published in Fizika Tverdogo Tela, 2010, Vol. 52, No. 8, pp. 1563–1569.

MAGNETISM AND FERROELECTRICITY

Digital Magnetic Heterostructures Based on Si and Fe

M. M. Otrokov[a, *], S. A. Ostanin[b], A. Ernst[b], V. M. Kuznetsov[a], and E. V. Chulkov[c, d]

[a] *Tomsk State University, pr. Lenina 36, Tomsk, 634050 Russia*

** e-mail: otrokov@phys.tsu.ru*

[b] *Max-Planck-Institut für Mikrostrukturphysik, Weinberg 2, Halle, D-06120 Germany*

[c] *Donostia International Physics Center (DIPC), Paseo Manuel de Lardizabal 4, Donostia–San Sebastián, Basque Country, 20018 Spain*

[d] *Departamento de Física de Materiales and Centro de Física de Materiales (CFM) CSIC–Universidad del País Vasco/Euskal Herriko Unibertsitatea (University of the Basque Country), Facultad de Ciencias Químicas, Universidad del País Vasco/Euskal Herriko Unibertsitatea (University of the Basque Country) Barrio Sarriena s/n, Donostia–San Sebastián, Basque Country, 48940 Spain*

Received November 18, 2009

Abstract—This paper reports on the results of *ab initio* calculations of the electronic and magnetic properties of Si digital heterostructures doped with a Fe monolayer of the substitutional or interstitial type. It has been revealed that, after the structural relaxation, heterostructures of both types exhibit a two-dimensional metallic behavior and a ferromagnetic ordering in the range of Si spacer thicknesses up to 19 atomic layers. The magnetization and spin polarization at the Fermi level for the heterostructures with an Fe monolayer of the substitutional type are two times higher than those for the system with an Fe monolayer of the interstitial type.

DOI: 10.1134/S1063783410080184

1. INTRODUCTION

Experimental and theoretical investigations of magnetic semiconductors are one of the most important fields of condensed matter physics from both technological and fundamental points of view. Magnetic semiconductors make it possible to control not only the charge of carriers, which underlies electronics, but also the spin of charge carriers. Therefore, they can have various applications. The majority of modern investigations in this field have been devoted to the study of GaAs-based systems. However, magnetic materials based on Si can appear to be more useful in practice, because it is Si that is the main material of electronics. The study of magnetic materials that can be easily integrated with Si electronic materials seems to be a very important problem. In this respect, *ab initio* investigations are growing in significance, which is especially evident for the so-called digital magnetic heterostructures (DMH) that consist of monolayers of magnetic transition metals in semiconductor films [1]. The DMH based on delta doping allow one to achieve magnetic impurity concentrations in semiconductors that considerably exceed the equilibrium solubility limit. The high degree of ordering of DMH and the perfectness of interfaces favor magnetic ordering. In the ferromagnetic (FM) case, the high concentration of magnetic atoms leads to a considerable increase in the Curie temperature [2]. Moreover, as follows from *ab initio* calculations, the DMH can have a higher spin polarization as compared to conventional ferromagnets [3–5], thus representing ideal materials for spin injection. The corresponding heterostructures have already been prepared experimentally in GaAs/Mn [2, 6] and GaSb/Mn [7, 8] materials.

At present, investigations of Si DMH have been predominantly associated with the doping by manganese because of its considerable magnetic moment, i.e., approximately $2.3\mu_B$ in the α structure (see theoretical studies in [4, 5] and experimental investigations in [9]). Since Fe atoms also have a substantial magnetic moment ($2.2\mu_B$ in the α (body-centered cubic) structure), it is also expedient to investigate DMH based on Si and Fe. Recently, Uspenskii and Kulatov [10] investigated the discrete magnetic heterostructure consisting of the Fe monolayer in Si by using the augmented plane wave method in the generalized gradient approximation to the exchange–correlation functional. The Fe monolayer was formed by means of the substitution of Fe atoms for Si atoms. In [10], it was demonstrated that, per two Fe atoms, the antiferromagnetic (AFM) configuration is more favorable than the FM configuration by 30 meV. It should be noted that no structural relaxations were performed in [10], even though their inclusion can result in a change in the "magnetic behavior" of the discrete magnetic heterostructure.

Up to now, Si/Fe heterostructures with an interstitial monolayer (Fe atoms occupy tetrahedral interstices in the Si lattice) have never been investigated. Therefore, in this work, we present the *ab initio* inves-

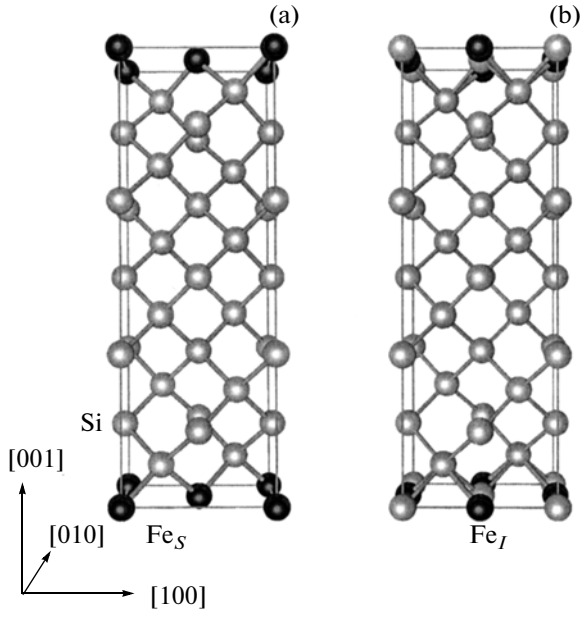

Fig. 1. Unit cells of Si heterostructures with an Fe monolayer of (a) the substitutional type Si_N/Fe_S and (b) the interstitial type Si_N/Fe_I for $N = 11$. The figure was prepared with the Balls and Sticks program [11].

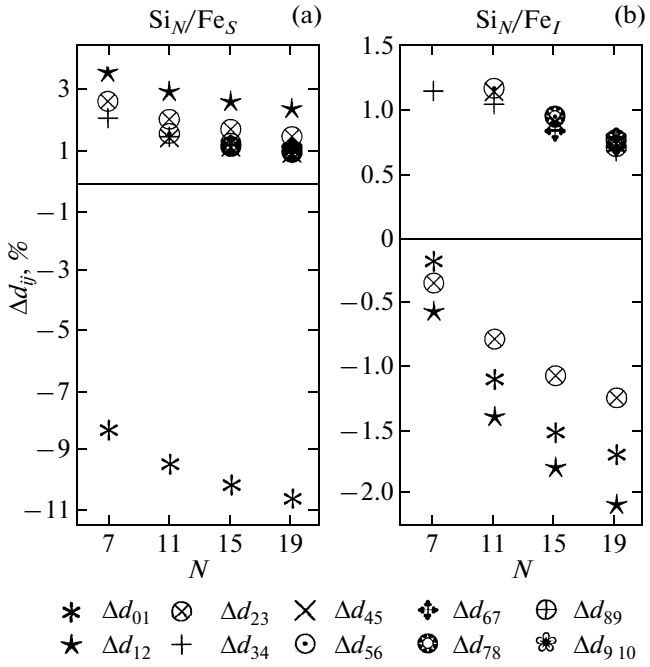

Fig. 2. Relative changes in the interplanar distances Δd_{ij} after the performance of the structural relaxation in the (a) Si_N/Fe_S and (b) Si_N/Fe_I systems. The Fe monolayer has number 0.

tigation of the electronic structure and magnetic properties of Si DMH doped with an Fe monolayer of the substitutional (Fe_S) or interstitial (Fe_I) type with taking into account the structural relaxations.

2. DESCRIPTION OF THE MODEL AND COMPUTATIONAL METHOD

The DMH were simulated using Si_N/Fe_S and Si_N/Fe_I supercells, which consisted of an Fe monolayer and a Si spacer with the thickness varying from $N = 7$ to 19 atomic layers. The basis vectors of the unit cell **a**, **b**, and **c** were directed along the [100], [010], and [001] axes, respectively, and their magnitudes were $a = b = a_0$ and $c = (N + 1)a_0/4$, where $a_0 = 5.46$ Å is the optimized lattice constant of bulk Si with a diamond structure. Figure 1 shows the Si_{11}/Fe_S and Si_{11}/Fe_I heterostructures. The calculations were performed in the framework of the density functional theory in the generalized gradient approximation to the exchange–correlation energy [12] with the use of the plane-wave basis set and the projector-augmented wave (PAW) pseudopotentials [13], as implemented in the VASP code [14–17]. The relaxation was carried out using the basis set of plane waves with energies <500 eV and the $6 \times 6 \times N_z$ Γ-centered **k**-point mesh [18], where $N_z = 3, 2, 2$, and 1 for the DMH consisting of 8, 12, 16, and 20 layers, respectively. The use of the denser mesh $8 \times 8 \times N_z$ in the Brillouin zone leads to a change in the total energy by no more than 1 meV per atom. The structural relaxation was performed until the forces at each atom in the superlattice became <0.01 eV/Å. The densities of states were calculated using the $12 \times 12 \times N_z$ ($N_z = 6, 4, 3, 2$) meshes.

3. RESULTS AND DISCUSSION

3.1. Structural Relaxation

The results of the calculations of the structural relaxation in the Si_N/Fe_S and Si_N/Fe_I systems along the [001] direction are presented in Fig. 2. In the course of relaxation, each plane of the (001) type moves as a whole (intraplanar atomic displacements along the [001] direction are negligible and are of the order of 10^{-2}%), whereas the plane containing the Fe monolayer and the $(N + 1)/2$th Si atomic layer remain fixed due to the periodicity of the cell. It can be seen from Fig. 2a that, during the relaxation in all Si_N/Fe_S systems, the distance Δd_{01} between the Fe_S monolayer and the nearest Si layers decreases. With an increase in N from 7 to 19, the quantity Δd_{01} decreases from −8.3 to −10.5%. In this case, the Fe–Si interatomic distance is approximately equal to 2.28 Å, which is very close to the experimentally observed distance Fe–Si equal to 2.29 Å in the *B*20 structure [19]. The interatomic distance specified for the Fe–Si pair before the relaxation (it corresponds to the distance between the nearest neighbors in perfect Si) in our calculations

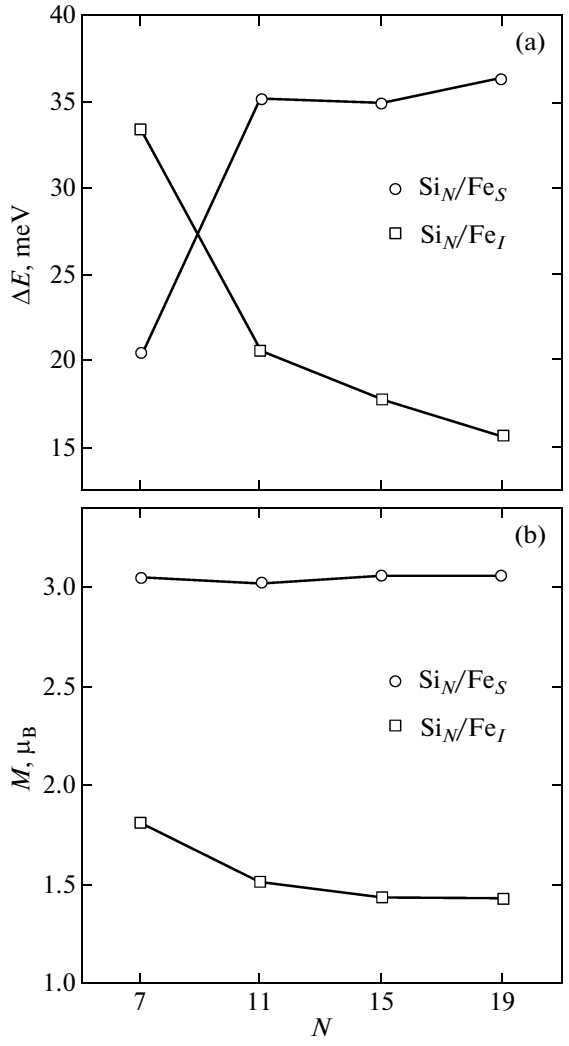

Fig. 3. (a) Difference between the energies of the AFM and FM configurations $\Delta E = E_{AFM} - E_{FM}$ per two Fe atoms as a function of the spacer thickness N. (b) Dependences of the net magnetic moment for the Si_N/Fe_S and Si_N/Fe_I FM configurations.

amounts to 2.36 Å. Therefore, the decrease in the distance between the Fe_S monolayer and the nearest Si atomic planes in the Si_N/Fe_S system is associated with the formation of the chemical bond length between the Fe and Si atoms. These atoms tend to form the bond with the length close to the length of the bond length between the same atoms in the conventional FeSi compound. Figure 2b illustrates the relaxation in the system with the Fe_I monolayer. It can be seen from this figure that the changes in the interplanar distances during the relaxation are considerably smaller than those in the system with the substitutional monolayer: $\Delta d_{01} = -1.7\%$ for the spacer thickness $N = 19$. Most likely, these insignificant relaxations are a simple consequence of the fact that the addition of Fe atoms to tetrahedral interstitials (actually, the addition of the material to a fixed volume) inevitably leads to the repulsion of the neighboring layers. This effect competes with the mechanism of formation of a shortened bond length between the Fe and Si atoms. Nonetheless, an increase in the spacer thickness results in an increase in the interplanar displacements. It is evident that the stresses caused by the incorporation of the Fe monolayer are redistributed between a larger number of layers in the heterostructure and the tendency of the Fe and Si atoms toward the formation of the bond with the length close to the bond length in the bulk FeSi compound is enhanced.

3.2. Magnetic Ordering

It can be seen from Fig. 3a that, for Si spacer thicknesses $7 \le N \le 19$, both systems Si_N/Fe are ordered ferromagnetically. It is interesting to note that the quantity ΔE changes substantially in the range from $N = 7$ to 11 layers and then varies rather weakly with a further increase in the spacer thickness. This indicates that the observed ferromagnetism has a two-dimensional character, because the contribution of spacer exchange interaction to the total energy becomes negligible for $N \ge 11$. Consequently, the formation of the FM order is determined by the direct exchange interaction between electrons of Fe atoms of the same monolayer, which are located at a distance of 3.86 Å from each other. Since the magnetic interactions along the [001] direction are weak, no change in the magnetic order in the ranges of thicknesses N (7, 11), (11, 15), and (15, 19) is expected in the Si_N/Fe systems. Previously, Uspenskii and Kulatov [10] investigated the DMH based on different semiconductors (Si, Ge, GaAs, GaSb, GaN) and transition metals (Cr, Mn, Fe, Co) and revealed that the Si/Fe_S system is antiferromagnetically ordered and that $\Delta E = -30$ meV per two Fe atoms. All DMH were studied without performing structural relaxations and only for one spacer thickness equal to 23 layers for the DMH with a diamond structure. Actually, in some cases, the inclusion of the structural relaxation does not lead to a qualitative change in the behavior of the system and, hence, can be omitted, for example, in Si/Mn_S [4], where the distance d_{01} changes insignificantly. However, the delta doping of Si with Fe with the substitutional type results in a decrease in the distance d_{01} by ~10%, which substantially affects the type of magnetic ordering.

3.3. Electronic Structure

In crystalline Si, with a diamond structure, the substitutional defects Fe_S and the interstitial defects Fe_I are located in the tetrahedral environment of four Si nearest neighbors. In this case, the fivefold degenerate d levels of Fe atoms are split by the crystal field into the doubly degenerate level e and the triply degenerate level t_2 [20]. The electronic orbitals of the Fe atoms

and their Si nearest neighbors are hybridized. According to the molecular orbital theory, the hybridization can occur only for states with identical symmetry [21]; in our case, these are the Si $t_2(p)$ and Fe $t_2(d)$ states.

The total and partial densities of states (DOS) calculated for the Si_{19}/Fe_S and Si_{19}/Fe_I systems are shown in Fig. 4. The DOS for the other Si_N/Fe_S and Si_N/Fe_I systems, except for specially noted differences, are very similar to those shown in Fig. 4 and, therefore, are not presented in our work. As can be seen from Fig. 4a (see the upper panel), the Si_{19}/Fe_S system exhibits a metallic DOS with the spin polarization at the Fermi level $P = |n\uparrow - n\downarrow|/(n\uparrow + n\downarrow) = 0.6$ (or 60%), where $n\uparrow = n\uparrow(E_F)$ and $n\downarrow = n\downarrow(E_F)$ are the differential DOS for spins up and spins down, respectively. In the majority-spin channel (solid lines), the states in the valence band between –2.5 and 1.0 eV are characterized by a strong Fe d–Si(1) p hybridization, which leads to "metallization" of local DOS of the Si atoms of the nearest layers (see panels Fe $t_2(d)$ and Si(1), Si(2), etc.). A considerable contribution to the valence band is also made by the $e(d)$ states located 1.5 eV below the Fermi level. In the vicinity of the upper edge of the valence band, the contributions of the Fe d states and Si p states are insignificant, which results in a low total DOS at the Fermi level in the majority-spin channel. In the conduction band, the fraction of the Fe d states with spin up is negligible and the contribution of the Si s and Si p states increases away from the Fermi level ($E > E_F$) (compare panels Total and Si(bulk) in Fig. 4a). In the minority-spin channel (dotted lines), the largest contribution to the conduction band in the range 0.5 eV above the Fermi level is made by the Fe $e(d)$ orbitals. It is these Fe $e(d)$ orbitals that provide a high spin polarization of the Si_{19}/Fe_S discrete magnetic heterostructure at the Fermi level, because the total DOS in the vicinity of the upper edge of the valence band of the minority-spin channel is rather low. The $t_2(d)$ orbitals make a smaller contribution to the DOS at the Fermi level, because they are predominantly located in the range 2 eV below the Fermi level E_F, where the Fe d–Si(1) p hybridization is also strong. Each Fe_S atom has a magnetic moment equal to $1.53\mu_B$. The magnetic moments induced at the four nearest atoms Si(1) are negative and amount to $-0.06\mu_B$, the magnetic moments of the Si(2) atoms of the second coordination sphere are equal to $0.02\mu_B$, and the magnetic moments of the father atoms located in the subsequent layers are smaller than $0.01\mu_B$. With allowance made for a magnetic moment of $0.13\mu_B$ outside the Wigner–Seitz spheres, the net magnetic moment per unit cell is equal to $3.06\mu_B$ (Fig. 3b).

The DOS for the Si_{19}/Fe_I system are shown in Fig. 4b. The partial DOS in the range from –3 to 1 eV for both spin channels are characterized by a strong hybridization of the Fe d states with the p states of the Si(1), Si(2), and Si(0) atoms, to which the distances are equal to 2.35, 2.65, and 2.73 Å, respectively. In this case, the partial densities of $t_2(d)$ and $e(d)$ states acquire a more "volume-like" form as compared to those for the Si_{19}/Fe_S system (compare, for example, the pronounced peak of the $e(d)$ states for the Si_{19}/Fe_S system and wide bands of the $e(d)$ states for the Si_{19}/Fe_I system in the minority-spin channels). In combination with an insignificant exchange splitting of the Fe d states, this leads to the following results: (1) a relatively low (of the order of 20%) spin polarization at the Fermi level and (2) a decrease in the magnetic moment at the Fe_I atoms (as compared to the Si_{19}/Fe_S system) to $0.71\mu_B$. As a consequence, the magnetic moments induced at the nearest Si atoms are small (less than $0.01\mu_B$). With due regard for a magnetic moment of $0.01\mu_B$ outside the Wigner–Seitz spheres, the net magnetic moment per unit cell is equal to $1.43\mu_B$ (Fig. 3b). The factor responsible for the broadening of the Fe d bands in the interstitial monolayer lies in a closer location of atoms and, hence, in a stronger interatomic interaction as compared to that in the plane of the Fe_S monolayer. Actually, in the case of the substitutional monolayer, the first neighbor of the Fe atom in the monolayer plane is also the Fe atom located at a distance of 3.86 Å. In the interstitial monolayer, the distance between the Fe atoms is also equal to 3.86 Å, but the Si(0) atom is located at a distance of 2.73 Å (Fig. 1). Therefore, the atomic density in the plane containing the interstitial monolayer is higher than that in the substitutional layer plane. As a result, the arising higher electron concentration leads to a stronger interatomic interaction and hybridization of bands. The decrease in the exchange splitting of the Fe_I d subband as compared to the exchange splitting of the Fe_S d subband can be understood using the following simple explanation. The exchange splitting of the Fe d levels in the Si_{19}/Fe_S system is smaller than that in body-centered cubic Fe, because the nearest neighbors of Fe atoms in the discrete magnetic heterostructure are nonmagnetic Si atoms. Since four additional nonmagnetic neighbors, i.e., Si(0) atoms, appear for the Fe atom in the Si_{19}/Fe_I system, the exchange splitting of its d levels becomes even smaller.

It should be noted that, in both the Si_{19}/Fe_S system and the Si_{19}/Fe_I system, all Si atoms of the first seven layers (the reference point corresponds to the Fe monolayer) make a contribution to the DOS in the region of the fundamental band gap. This contribution decreases with an increase in the distance from the Si atoms to the Fe monolayer. Beginning with the eighth layer, the local DOS for the Si atoms exhibit a band gap of approximately 0.6 eV and the form corresponding to that of the local DOS of intrinsic bulk Si (see panel Si(bulk)). Consequently, both types of the DMH under consideration represent two-dimensional metals. It is clear that their conductivity along the [001]

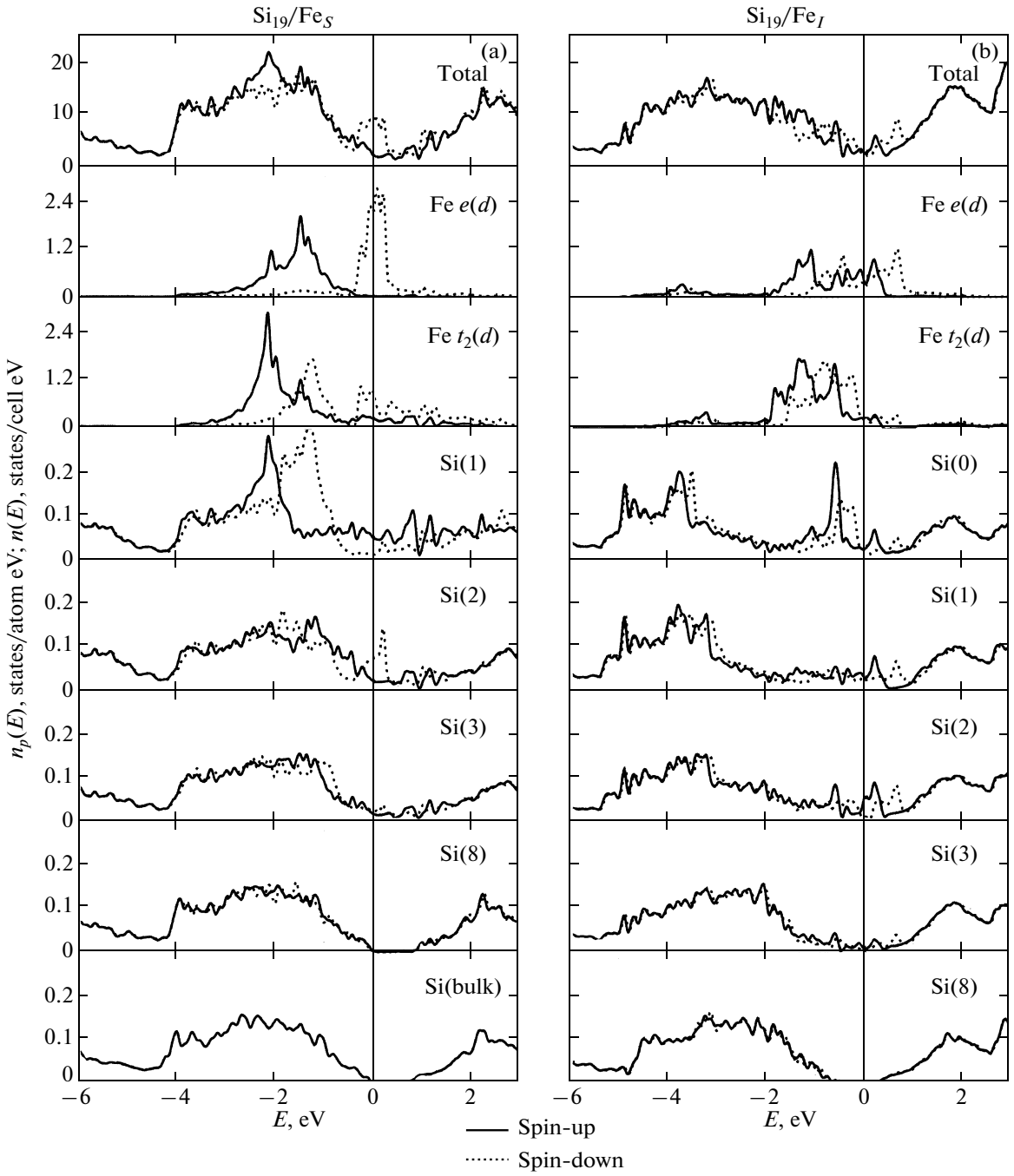

Fig. 4. Calculated total $n(E)$ and partial $n_p(E)$ DOS for the (a) Si_{19}/Fe_S and (b) Si_{19}/Fe_I systems. The Fermi level corresponds to zero energy. The Si(1), Si(2), Si(3), and Si(8) atoms are the Si atoms in the layers with numbers 1, 2, 3, and 8, respectively (the reference point corresponds to the Fe monolayer). For the Si_{19}/Fe_I system, Si(0) indicates the atom located in the plane of the Fe_I monolayer. The Si(bulk) atom corresponds to the atom in intrinsic bulk Si with a diamond structure (in this case, the shown partial DOS is not spin-polarized). Partial DOS for all Si atoms represent the summarized contribution of the *s* and *p* states in the corresponding spin channels inside the Wigner–Seitz spheres.

direction is considerably lower than the conductivity in the plane doped with Fe. This property is retained for the DMH with thin Si spacers. Although, at $N = 7$, none of the Si atoms have a DOS with a pronounced band gap, the conductivity of these DMH in the direction perpendicular to the monolayer plane, as before, is substantially lower than that along this plane.

Figure 5 shows the band structures for the Si_{19}/Fe_S and Si_{19}/Fe_I systems along the Γ–X–M–Γ–Z symme-

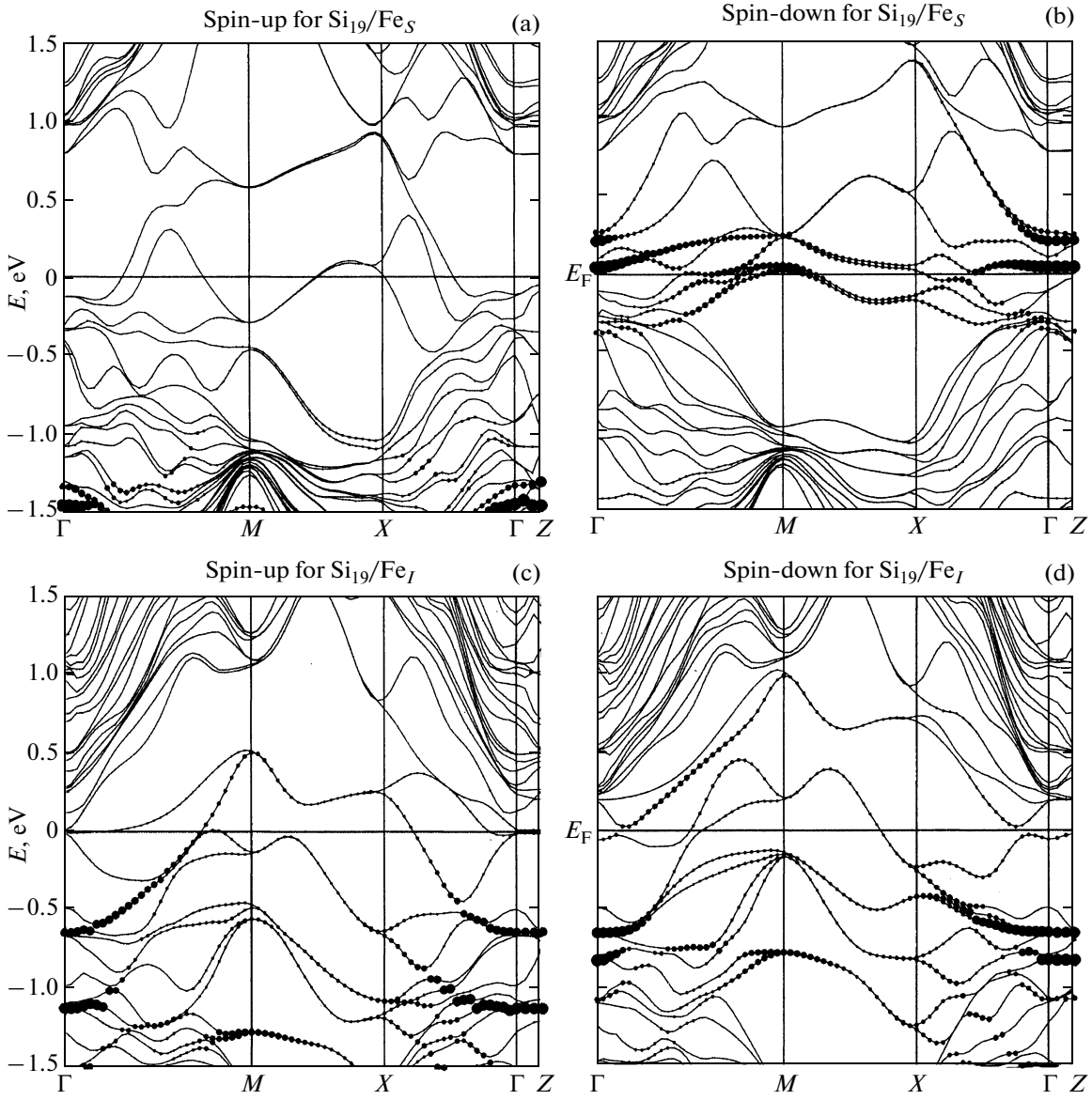

Fig. 5. Spin-polarized band structures of the (a, b) Si_{19}/Fe_S and (c, d) Si_{19}/Fe_I systems along the $\Gamma-M-X-\Gamma-Z$ direction of the Brillouin zone. The coordinates of the symmetry points of the Brillouin zone are as follows: $\Gamma = (0, 0, 0)$, $M = (0.5, 0.5, 0)$, $X = (0.5, 0, 0)$, and $Z = (0, 0, 0.5)$. The size of symbols reflects the relative fraction of the *d* states at the given **k** point.

try directions in the Brillouin zone. The $\Gamma-X-M-\Gamma$ and $\Gamma-Z$ directions, which lie in the $\mathbf{k}_x-\mathbf{k}_y$ and $\mathbf{k}_z$ planes of the Brillouin zone, respectively, describe the states in the plane of the Fe monolayer (i.e., in the (001) plane) and along the perpendicular [001] direction of the direct lattice. The size of symbols in the figures reflects the relative fraction of the *d* states. In the majority-spin channel for the Si_{19}/Fe_S system (Fig. 5a), three partially occupied bands provide a metallic conductivity. As was noted above, the states in the conduction band of the majority-spin channel are predominantly Si $t_2(p)$ in character, because the $e(d)$ and $t_2(d)$ states are located below the Fermi level (see panel Fe $t_2(d)$ in Fig. 4a). In the minority-spin channel, the conductivity also exhibits a metallic behavior. At the Fermi level and its vicinity, there are narrow bands in which the states are predominantly $e(d)$ in character (see panels Fe $e(d)$ and Fe $t_2(d)$ in Fig. 4). These states ensure a high spin polarization at the Fermi level of the system. Along the $\Gamma-Z$ direction, the larger the fraction of the *d* states in the $p-d$ hybridized bands, the higher their localization. This is a consequence of the specific structure of the discrete magnetic heterostructure: along the [001] direction, the profile of the dopant distribution is a delta function. Therefore, along the $\Gamma-Z$ direction, the narrow impu-

rity bands are located in contrast to the broadened bands located along the $\Gamma-X-M-\Gamma$ direction, which describe the states of electrons in the monolayer plane, where a two-dimensional metallic bonding appears. Moreover, in both spin channels, states at the Fermi level along the $\Gamma-Z$ direction are absent; the charge carriers are predominantly located in the vicinity of the Fe_S monolayer, which also confirms the two-dimensional metallic behavior of the system under consideration.

The metallic conductivity in the Si_{19}/Fe_I system is provided by three and two partially occupied bands in the majority-spin and minority-spin channels, respectively (Figs. 5c, 5d); in this case, it can be seen from Fig. 4b that the conduction band contains the states of both symmetries $e(d)$ and $t_2(d)$. In the $\mathbf{k}_x-\mathbf{k}_y$ plane (the $\Gamma-X-M-\Gamma$ directions), the extent of the $p-d$ hybridized bands is larger, on average, than that in the Si_{19}/Fe_S system, which indicates a more considerable interatomic interaction in the Fe_I monolayer. As regards the $\Gamma-Z$ direction, the bands with the dominance of the d character are also strongly localized, as is the case in the Si_{19}/Fe_S system, due to the delta profile of the dopant distribution in the [001] direction of the direct lattice. The Si_{19}/Fe_I system, like the Si_{19}/Fe_S system, has no states at the Fermi level along the $\Gamma-Z$ direction: the majority-spin channel has a pseudogap equal to 29 meV. This circumstance suggests that charge carriers are predominantly located in the vicinity of the Fe_I monolayer.

4. CONCLUSIONS

Thus, the N-layer Si DMH with an Fe layer of the substitutional or interstitial type have been investigated using *ab initio* calculations. It has been demonstrated that, in the study of the Si_N/Fe_S system, it is very important to account for the structural relaxation, because the difference between the energies of the FM and AFM configurations ΔE is sensitive to a change in the distance between the Fe_S monolayer and the nearest Si atomic planes. Both types of the doped systems are ferromagnetically ordered over the entire range of Si spacer thicknesses N under investigation. For $N \geq 11$, the DMH under consideration exhibit a two-dimensional FM order, which arises as a result of the direct exchange between the Fe atoms inside the monolayer. For $N = 7$, there can occur insignificant exchange interactions between the neighboring Fe monolayers, whereas, at $N \geq 11$, their contribution to ΔE is negligible. In view of the decrease in the exchange splitting, the d subbands with different spin directions in the Si_N/Fe_I systems more strongly overlap as compared to the Si_N/Fe_S systems. As a result, the net magnetic moment and the spin polarization in the Si_N/Fe_S systems exceed the corresponding quantities in the Si_N/Fe_I systems by a factor of more than two: $1.53\mu_B$ and 60% as compared to $0.71\mu_B$ and 20%, respectively. According to our calculations and the data available in the literature [3–5], the two-dimensional metallic behavior is a property in common for DMH irrespective of a specific semiconductor matrix and a delta doping transition metal. This means that, in these systems, the conductivity in the direction perpendicular to the monolayer plane is substantially lower than the conductivity along this plane, because charge carriers are predominantly located in the vicinity of the transition metal monolayer.

The calculations were performed on the SKIF Cyberia computational cluster at the Tomsk State University (Tomsk, Russia).

ACKNOWLEDGMENTS

We would like to thank S.V. Eremeev and I.A. Nechaev for helpful discussion.

This study was supported in part by the University of the Basque Country (project GV-UPV, grant no. IT-366-07) and the Spanish Ministerio de Ciencia y Tecnología (MCyT) (grant no. FIS2007-06671-C02-01).

REFERENCES

1. S. A. Crooker, D. A. Tulchinsky, J. Levy, D. D. Awschalom, R. Garcia, and N. Samarth, Phys. Rev. Lett. **75**, 505 (1995).
2. A. M. Nazmul, T. Amemiya, Y. Shuto, S. Sugahara, and M. Tanaka, Phys. Rev. Lett. **95**, 017201 (2005).
3. S. Sanvito, Phys. Rev. B: Condens. Matter **68**, 054425 (2003).
4. M. C. Qian, C. Y. Fong, K. Liu, W. E. Pickett, J. E. Pask, and L. H. Yang, Phys. Rev. Lett. **96**, 027211 (2006).
5. H. Wu, P. Kratzer, and M. Scheffler, Phys. Rev. Lett. **98**, 117202 (2007).
6. R. K. Kawakami, E. Johnston-Halperin, L. F. Chen, M. Hanson, N. Guébels, J. S. Speck, A. C. Gossard, and D. D. Awschalom, Appl. Phys. Lett. **77**, 2379 (2000).
7. X. Chen, M. Na, M. Cheon, S. Wang, H. Luo, B. D. McCombe, X. Liu, Y. Sasaki, T. Wojtowicz, J. K. Furdyna, S. J. Potashnik, and P. Schiffer, Appl. Phys. Lett. **81**, 511 (2002).
8. G. B. Kim, M. Cheon, S. Wang, H. Luo, B. D. McCombe, X. Liu, Y. Sasaki, T. Wojtowicz, and J. K. Furdyna, Physica E (Amsterdam) **20**, 355 (2004).
9. S. H. Chiu, H. S. Hsu, and J. C. A. Huang, J. Appl. Phys. **103**, 07D110 (2008).
10. Yu. A. Uspenskii and E. T. Kulatov, J. Magn. Magn. Mater. **321** (7), 931 (2009).

11. *Balls and Sticks: Program Designed to Create 3D-Pictures and Animations of Crystals* http://www.softbug.com/toycrate/bs/index.html; T. C. Ozawa and S. J. Kang, J. Appl. Crystallogr. **37**, 679 (2004).
12. J. P. Perdew and W. Wang, Phys. Rev. B: Condens. Matter **45**, 13244 (1992).
13. P. E. Blöchl, Phys. Rev. B: Condens. Matter **50**, 17953 (1994).
14. G. Kresse and J. Hafner, Phys. Rev. B: Condens. Matter **47**, 558 (1993); Phys. Rev. B: Condens. Matter **49**, 14251 (1994).
15. G. Kresse and J. Furthmüller, Comput. Mater. Sci. **6**, 15 (1996).
16. G. Kresse and J. Furthmüller, Phys. Rev. B: Condens. Matter **54**, 11169 (1996).
17. G. Kresse and J. Joubert, Phys. Rev. B: Condens. Matter **59**, 1758 (1999).
18. H. J. Monkhorst and J. D. Pack, Phys. Rev. B: Solid State **13**, 5188 (1976).
19. R. Wartchow, S. Gerighausen, and M. Binnewies, Z. Kristallogr.—New Cryst. Struct. **212**, 320 (1997).
20. F. A. Cotton, *Chemical Applications of Group Theory* (Wiley, New York, 1990).
21. S. Fudzinaga, *Method of Molecular Orbitals* (Iwanami Shoten, Tokyo, 1980; Mir, Moscow, 1983).

Translated by O. Borovik-Romanova